

# Non-reciprocal Scattering in a Microwave Frequency Comb

Christoph L. Bock, J. C. Rivera Hernández, Fabio Lingua, and David B. Haviland\*  
*Department of Applied Physics, KTH Royal Institute of Technology, SE-10691 Stockholm, Sweden*  
 (Dated: February 4, 2025)

We investigate non-reciprocal scattering within the modes of a microwave frequency comb. Adjusting the pump frequencies, amplitudes, and phases of a Josephson parametric oscillator, we control constructive interference for the  $m \rightarrow \ell$  scattering processes, while concurrently achieving destructive interference for the inverse process  $\ell \rightarrow m$ . We outline the methodology for realizing non-reciprocity in the context of two-mode isolation and a three-mode circulation, which we extend to multiple modes. We find good agreement between the experiments and a linearized theoretical model. Nonreciprocal scattering expands the toolset for parametric control, with the potential to engineer novel quantum correlations.

## I. INTRODUCTION

Microwave superconducting circuits have emerged as a leading platform for quantum technology [1–5]. A measurement of the quantum state of these circuits typically requires amplifiers that introduce excessive back-action and undesired decoherence. Measurement through non-reciprocal devices mitigates the back-action and is therefore considered essential to any microwave quantum technology. Achieving non-reciprocity in a compact and reconfigurable measurement scheme, which does not rely on bulky magnetic-based circulators, is highly desired. Josephson parametric amplifiers (JPAs) can in theory work at the quantum limit of back-action [6], but their typical mode of operation is reciprocal [7–12].

Significant effort has focused on Josephson junction devices for directional quantum-limited amplification [13–16] and non-magnetic circulation [17–19]. Non-reciprocal scattering was demonstrated in a passive Josephson junction ring [20], as well as non-reciprocal frequency conversion and amplification in a multi-modal Josephson circuit [21–23]. These solutions often require multiple coupled resonators and other components which constrain efficient signal routing, bandwidth, and tunability. Simplifying the circuitry while maintaining non-reciprocal behavior for tunable, selected bandwidths would greatly enhance the scalability and integration of quantum hardware.

This work explores the use of a single JPA to non-reciprocally connect input and output tones in a microwave frequency comb. We analyze non-reciprocity in the context of asymmetric scattering between these modes [24, 25]. Multiple low and high-frequency pumps with carefully tuned amplitude and phase enable non-reciprocity. We explore different non-reciprocal scattering regimes, ranging from two-mode isolation and three-mode circulation to a general non-reciprocal scattering between  $n = 41$  modes. Our scattering approach represents a first step toward a compact, scalable, and reconfigurable non-reciprocal measurement scheme for mi-

crowave quantum technology.

## II. SETUP AND EXPERIMENT

The experiments measure the scattering of a weak input signal that intermodulates with a multifrequency pump waveform, producing multiple intermodulation products called idlers. The JPA consists of a lumped-element LC circuit, incorporating a gradiometric superconducting quantum interference device (SQUID) whose inductance is modulated by an external time-dependent signal applied through the pump port (see Fig. 1). A DC bias at the pump port tunes the resonant frequency of the JPA to  $\omega_0 = 2\pi \times 4.2$  GHz. The signal port is over-coupled, yielding a loaded quality factor  $Q = 37.5$ , corresponding to a linewidth  $\kappa = 2\pi \times 112$  MHz. A circulator separates the input and output signals, directing the output to a cryogenic low-noise amplifier.

A digital multifrequency lock-in amplifier [26] generates the pump tones and the weak coherent signal while demodulating at up to 192 frequencies. We chose all pump, signal, and demodulation tones from a mode basis  $\{a_m\}$  whose frequencies are integer multiples of the measurement bandwidth  $\Delta = 1/T = 2\pi \times 125$  kHz, where  $T$  is the measurement time window. This choice ensures orthogonality of the modes  $\{a_m\}$  and establishes a global phase reference for modulation and demodulation. We further eliminate Fourier leakage between demodulated modes by tuning  $\Delta$  to be commensurate with the digital sampling frequency. The enumeration scheme for the mode frequencies is  $\omega_m = \omega_0 \pm m\Delta$ ,  $m \in \mathbb{N}$ , with the center frequency  $\omega_0$  placed within  $\Delta$  of the resonant frequency of the JPA.

We synthesize the multifrequency pump waveform by superposing tones selected from the same basis  $\{a_m\}$ , distinguishing between low- and high-frequency pump tones. Low-frequency pumps have  $\Omega_k = k\Delta$ , while high-frequency pumps have  $\Omega_k = 2\omega_0 \pm k\Delta$ , where  $k$  is a small positive integer. The synchronous low and high-frequency pumps are output through different ports of the multifrequency lock-in amplifier and combined at the mixing chamber using a diplexer, as shown in Fig. 1.

\* haviland@kth.se



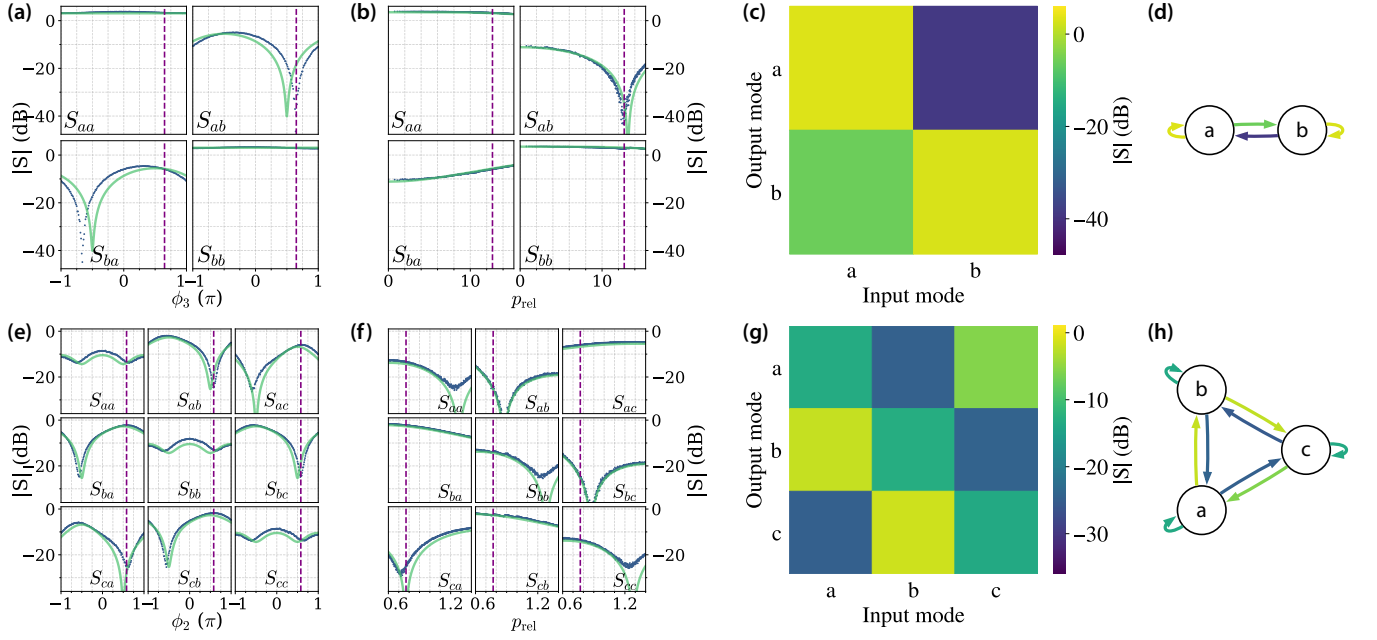


FIG. 2. (a)-(d) Isolator. (e)-(h) Circulator. (a) and (e) Scattering parameters as a function of the phase  $\phi_3$  and  $\phi_2$  for fixed pump powers, respectively. (b) and (f) Scattering parameters as a function of the relative amplitude  $p_{rel}$  for fixed phases. Blue dots refer to experimental data and green lines to numerical solutions. (c) and (g) Measured scattering matrix at the optimal amplitude and phase values given by the vertical dashed lines. (d) and (h) Graph representation of the scattering matrix.

6 dB of insertion loss. Reprogramming the pump waveform to  $\phi_3 = -0.67\pi$  reverses the direction of isolation, without physically changing the circuit or connection ports. In Fig. 2(c) we plot the scattering matrix at the optimal values  $\phi_3$  and  $p_{rel}$ . The directed graph in Fig. 2(d) summarizes the isolator, with arrows color-coded according to the  $S$ -parameters.

We find qualitative agreement between the experimental results and the numerical solution of the equations of motion, as shown by the green lines in Fig. 2(a) and (b). We find a discrepancy between the experimental and theoretical value of the phase  $\phi_3$  for destructive interference, that we attribute to nonlinearity in the experiment which is not accounted for in the theoretical model. We analyze the interference process between  $S_{ab}$  and  $S_{ba}$  using the graphical Cramer method [25, 29] (see Appendix A for details). For the isolator, the mode couplings, determined by the pumping scheme, are illustrated in Fig. 3(a), with a detailed discussion provided in Appendix A 1.

The exact expansion of  $S_{ab}$  and  $S_{ba}$  is shown in Fig. 3(b). The diagonal elements of the matrix  $\mathbf{M}$ , denoted as  $\Delta_m = -\omega_m - \omega_0 + i\gamma/2 = \kappa_m e^{i\alpha_m}$ , encode information about the frequency and losses of the mode  $m$ , while  $-\Delta_m^*$  encode the anti-mode.  $S_{ab} = 0$  arises from the destructive interference between the second-order intermodulation product involving the pump at  $\Omega_3$  and the third-order intermodulation products involving the pumps at  $\Omega_1$  and  $\Omega_2$ .

To match the experimental conditions, we assume equal strengths for the high-frequency pumps ( $|g_1| =$

$|g_2| = g$ ) and a relative strength for the low-frequency pump ( $|g_3| = rg$ , with  $r \in \mathbb{R}$ ). Setting  $S_{ab} = 0$  we arrive at the condition for perfect destructive interference,

$$g^2 = rg\kappa_d \equiv \rho, \quad (5)$$

$$\phi_{loop} = -\alpha_d \quad (6)$$

where  $\phi_{loop} = \phi_1 - \phi_2 + \phi_3$  is the total phase of the loop between the three interfering pumps shown in blue in Fig. 3(a). In our experiment we tune  $\phi_1 = \phi_2$  resulting in  $\phi_{loop} = \phi_3 = -\alpha_d$ . Substituting the conditions (5) and (6) into the expression for  $S_{ba}$ , we find  $S_{ba} \propto \rho(1 - e^{-2i\alpha_d})$ , which reaches a maximum when  $\phi_3 = \frac{\pi}{2}$ . The analytic expansion thus explains the non-reciprocal behavior observed in the experiment, which shows good agreement with the numerical solutions of the equations of motion.

## B. Three-mode non-reciprocal scattering: the circulator

Circulation is realized with two low-frequency pumps at  $\Omega_1 = \Delta$  and  $\Omega_2 = 2\Delta$ , which couple three modes at frequencies  $\omega_b$ ,  $\omega_a = \omega_b - \Delta$ , and  $\omega_c = \omega_b + \Delta$ . The interference between different orders of intermodulation that generate idlers at these three frequencies depends on the phase of either pump and their relative amplitude. Figure 2(e) shows the scattering as a function of  $\phi_2$  at a fixed value of  $p_{rel} = p_1/p_2 = 0.77$ . At  $\phi_2 = 0.58\pi$ , constructive interference enhances  $S_{ba}$ ,  $S_{ac}$ , and  $S_{cb}$ , while destruc-

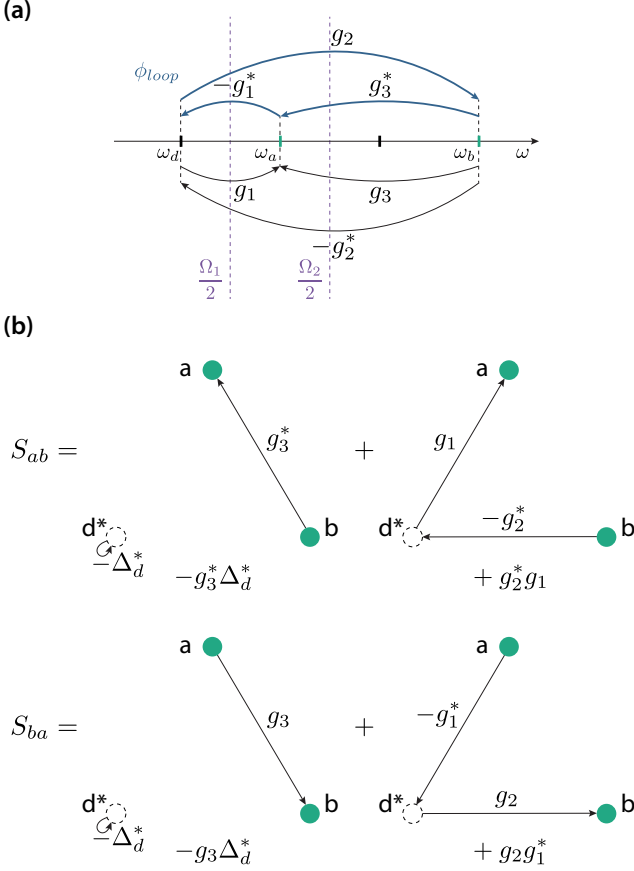


FIG. 3. Isolator mode coupling scheme (a), digraph expansion of scattering matrix elements  $S_{ab}$ ,  $S_{ba}$  (b).

tive interference suppresses  $S_{ca}$ ,  $S_{ab}$  and  $S_{bc}$ , establishing clockwise circulation between the modes,  $a \rightarrow b \rightarrow c \rightarrow a$ .

In Fig. 2(f) we sweep the relative pump amplitude while fixing  $\phi_2 = 0.58\pi$ . At  $p_{rel} = 0.77$ , we achieve balanced isolation  $S_{ca}$ ,  $S_{ab}$ ,  $S_{bc} \simeq -24$  dB, insertion loss  $S_{ac}$ ,  $S_{ba}$ ,  $S_{cb} \simeq -3$  dB, and reflection  $S_{aa}$ ,  $S_{bb}$ ,  $S_{cc} \simeq -13$  dB. At  $p_{rel} = 1.24$  we minimize reflection to  $-25$  dB at the cost of reducing and unbalancing isolation to  $S_{ca} \simeq -10$  dB and  $S_{ab}$ ,  $S_{bc} \simeq -19$  dB. Figure 2(g) illustrates the scattering matrix for balanced isolation. Figure 2(h) summarizes the circulation in a directed graph. Changing  $\phi_2$  to  $-0.58\pi$  reverses the direction of circulation.

The theoretical model shows similarly good agreement with the experimental results [see green lines in Fig. 2(e) and (f)]. To understand the mixing processes underlying the circulator's non-reciprocal behavior, we consider the five modes depicted in Fig. 4(a). With  $n = 5$  modes the full analytical Cramer method becomes impractical. However, approximate expressions for  $S_{ab}$  and  $S_{ba}$  can be derived by truncating the digraph expansion to higher-order terms in pump power. Figure 4(a) shows the couplings provided by the two low-frequency pumps. We define the couplings as  $g_1 = ge^{i/\phi_1}$  and  $g_2 = rge^{i/\phi_2}$ ,

with  $r = \frac{|g_1|}{|g_2|} \in \mathbb{R}$ , and assume  $g \ll 1$  to match the weak pump regime of our experiment (see appendix A 2). Figure 4(b) shows the digraph expansion of  $S_{ab}$  and  $S_{ba}$  to second-order in  $g$ , corresponding to the expressions

$$S_{ab} \simeq \frac{i\gamma}{|M|} (ge^{-i\phi_1} \Delta_d \Delta_e \Delta_c + r^2 g^2 e^{-i2\phi_2} \Delta_e \Delta_c + o(g^3)), \quad (7)$$

$$S_{ba} \simeq \frac{i\gamma}{|M|} (ge^{i\phi_1} \Delta_d \Delta_e \Delta_c + r^2 g^2 e^{i2\phi_2} \Delta_e \Delta_c + o(g^3)). \quad (8)$$

This expansion shows that the relevant interfering process comes from mixing products that involve the pump  $\Omega_1$  and twice the pump  $\Omega_2$ . Taking  $S_{ab} = 0$  we retrieve the conditions on the magnitude  $g\kappa_d = r^2 g^2 \equiv \rho$  and on the total phase of the loop of  $\phi_{loop} = 2\phi_2 - \phi_1 = -\alpha_d$  (blue loop in Fig. 4(a)). Setting  $\phi_1 = 0$  we derive

$$S_{ba} \propto \rho (e^{i\alpha_d} - e^{-i\alpha_d}) = 2i\rho \sin \alpha_d \neq 0, \quad (9)$$

which is generally non-zero because the diagonal elements  $\Delta_m$  contain the losses  $\gamma$  due to coupling to the transmission line. Similar arguments can be extended to higher-order terms ( $O(g^3)$ ) to prove non-reciprocal scattering between modes  $a$  and  $c$ . Details are provided in Appendix A 2.

This analytical approximation confirms the circulation behavior shown in the experimental and numerical results. Whenever the condition  $S_{ab} = S_{bc} \simeq S_{ca} \simeq 0$  holds,  $S_{ba} = S_{cb} \simeq S_{ac} \neq 0$  holds.

### C. n-mode non-reciprocal scattering

We extend the isolator and circulator schemes to achieve non-reciprocal scattering across  $n = 41$  modes. We measure the scattering of a coherent tone stepped through the mode basis  $\{a_m\}$  while simultaneously listening at all frequencies.

Top panels of Fig. 5 show the measured scattering matrix, normalized to the zero-pump case, for two high-frequency pumps at  $\Omega_{1,2} = 2\omega_0 \pm 2\Delta$ , and a low-frequency pump at  $\Omega_3 = 4\Delta$ , as in the two-mode isolator configuration. We fix the pump amplitudes and phases according to the optimal parameters in the two-mode isolator to cancel the first upper diagonal in  $\mathbf{S}$ , allowing transmission along the lower diagonal. Adjusting the phase to  $\phi_3 = -0.67\pi$  cancels the lower diagonal while transmitting the upper diagonal.

Bottom panels of Fig. 5 show the normalized  $\mathbf{S}$  matrix for two low-frequency pumps at  $\Omega_1 = 2\Delta$  and  $\Omega_2 = 4\Delta$ , following the three-mode circulator scheme. The  $\mathbf{S}$  matrix reveals an imbalance between the upper and lower diagonals, demonstrating non-reciprocity. However, we do not observe circulation between all  $n = 41$  modes,

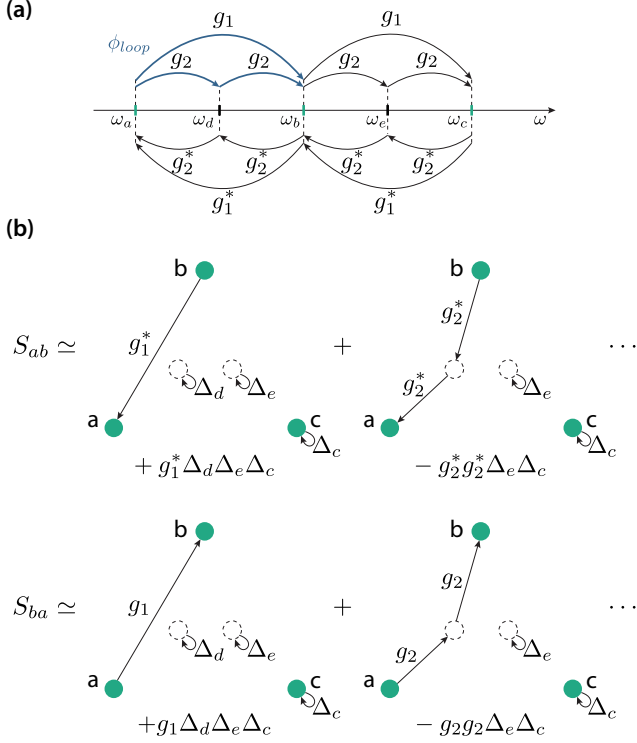


FIG. 4. Circulator mode coupling scheme (a), second order digraph expansion of scattering matrix elements  $S_{ab}$ ,  $S_{ba}$  (b).

likely due to increased complexity and overlapping scattering pathways.

Theoretical scattering matrices align well with the experimental results, as shown in Fig. 5. We find optimal parameters for the effective transmission line coupling  $\gamma$ , pump amplitudes  $p_k$ , and pump phases  $\phi_k$  that minimize the sum of the element-wise square distance between the numerical and measured scattering matrices.

#### IV. CONCLUSION

We studied the non-reciprocal scattering of a JPA in different regimes. We defined non-reciprocity in terms of asymmetry in scattering magnitude between input and output frequency modes. Pumping the JPA with a combination of low and high-frequency pumps, we realized different non-reciprocal behavior ranging from two-mode isolation to three-mode circulation. The presence of multiple pumps creates a multitude of three and four-wave mixing processes (second and third-order intermodulation) connecting the input signal to a given idler. By carefully tuning pump frequencies, phases, and amplitudes we create destructive interference for processes  $m \rightarrow \ell$  while simultaneously creating constructive interference for the inverse  $\ell \rightarrow m$  processes. We provided a general recipe for non-reciprocity extending the case of a two-mode isolator to a measurement basis of  $n = 41$

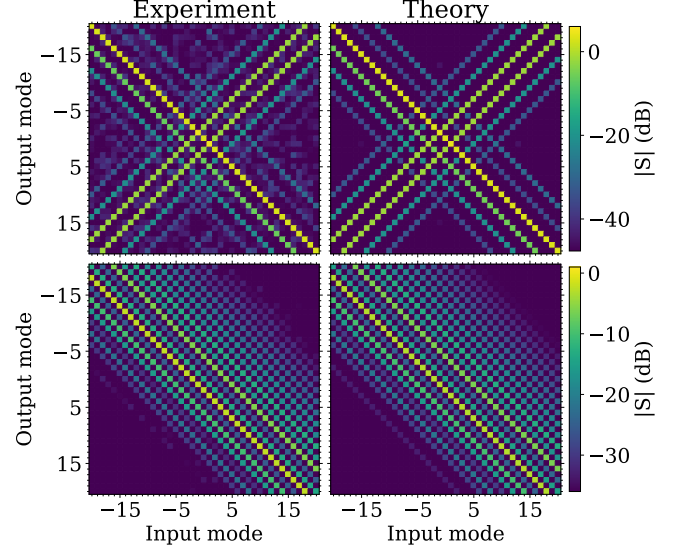


FIG. 5. Experimental (left) and theoretical (right) scattering matrices. The upper (lower) panels correspond to pumping the JPA with two high and one low-frequency (two low-frequency conversion) pumps. The magnitude of the scattering is expressed in dB, normalized to the pump-off case.

modes, with good agreement between experiment and theory. This approach constitutes a new building block in the toolset of parametric control, with the ability to easily reconfigure non-reciprocal mode scattering.

#### ACKNOWLEDGMENTS

We acknowledge Joe Aumentado and John Teufel at the National Institute of Standards and Technology (NIST) for helpful discussions and for providing the JPA used in this experiment. We also acknowledge fruitful discussions with Kirill Petrovnnin, Ilari Lilja, Ekaterina Mukhanova, and Pertti Hakonen at Aalto University. This work was supported by the Knut and Alice Wallenberg Foundation through the Wallenberg Center for Quantum Technology (WACQT).

#### AUTHOR DECLARATION

#### Conflict of interest statement

D. B. H. is part owner of the company Intermodulation Products AB, which produces the digital microwave platform used in this experiment.



## Author contributions

## DATA AVAILABILITY

After review, data will be made available on Zenodo.

## Appendix A: Analytical analysis of scattering

As mentioned in the main text, the equations of motion (2) can be written in the matrix form

$$-i\mathbf{M}\vec{a} = \sqrt{\gamma}\vec{a}_{\text{in}}, \quad (\text{A1})$$

where  $\mathbf{M}$  is a  $2n \times 2n$  matrix and takes the general form

$$\mathbf{M} = \mathbf{M}_0 + \sum_k \mathbf{G}_k. \quad (\text{A2})$$

Here  $\mathbf{M}_0$  is a  $2n \times 2n$  diagonal matrix containing the mode frequencies

$$\mathbf{M}_0 = \begin{pmatrix} \Delta_{-\frac{n}{2}} & & & & \\ & -\Delta_{-\frac{n}{2}}^* & & & \\ & & \ddots & & \\ & & & \Delta_{\frac{n}{2}} & \\ & & & & -\Delta_{\frac{n}{2}}^* \end{pmatrix}, \quad (\text{A3})$$

where an element  $\Delta_m = -\omega_m - \tilde{\omega}_0 \in \mathbb{C}$ , while the  $\mathbf{G}_k$  are  $2n \times 2n$  coupling matrices due to pump  $k$ . The non-zero elements  $m\ell$  of each matrix  $\mathbf{G}_k$  couple modes  $m$  and  $\ell$  through pump  $k$ , in direct proportion to the complex amplitude  $g_k = p_k e^{i\phi_k}$ . For low-frequency pumps, where  $\Omega_k = k\Delta$ , we have

$$\mathbf{G}_k = \begin{pmatrix} 0 & & g_k & & \\ & 0 & & -g_k^* & \\ & & \ddots & & \ddots \\ g_k^* & & & 0 & g_k \\ -g_k & & & & 0 & -g_k^* \\ & \ddots & & & \ddots & \\ & & g_k^* & & 0 & \\ & & & -g_k & & 0 \end{pmatrix}, \quad (\text{A4})$$

with two non-zero off-diagonals at position  $\pm k$ . For high-frequency pumps, where  $\Omega_k = 2\omega_0 + k\Delta$ , we have

$$\mathbf{G}_k = \begin{pmatrix} 0 & & & g_k & & \\ & 0 & & & -g_k^* & \\ & & \ddots & & & \ddots \\ & & & \ddots & & \\ g_k & & & & 0 & \\ -g_k^* & & & & & 0 & & \ddots & 0 \end{pmatrix}, \quad (\text{A5})$$

with one non-zero anti-diagonal in position  $k$ .

Solutions to Eq. (A1) are readily available by inverting the matrix  $\mathbf{M}$ , with the scattering matrix given by Eq. (3). For a small number of modes, one can analytically compute  $\mathbf{M}^{-1}$  following the graphical Cramer method used in [25, 29]. This diagrammatic method computes the determinant of  $\mathbf{M}$  and the elements of  $\mathbf{M}^{-1}$  by summing weighted directed graphs, called *digraphs*. Digraph vertices represent modes, while edges correspond to mode couplings induced by the pumps.

The determinant of  $\mathbf{M}$  is computed by summing *all* possible digraphs, while the matrix element  $M_{m\ell}^{-1}$  is the sum of those digraphs with a path from mode  $\ell$  to  $m$  (see Fig. 3 for an example). The elements of the scattering matrix are

$$S_{m\ell} = \frac{i\gamma}{|\mathbf{M}|} \sum_{\ell \rightarrow m}^{\text{paths}} (-1)^{2n+l} M_{\ell,i_1} \dots M_{i_{n-4},m} - \delta_{m\ell}, \quad (\text{A6})$$

where the sum runs over all the possible paths from mode  $\ell$  to  $m$ , each with  $2n - 1$  edges. The paths are defined by the product of edges  $M_{\ell,i_1} M_{i_2,i_3} \dots M_{i_{n-4},m}$  through permutation of the indices  $\{m, i_1, \dots, i_{2n-4}, \ell\}$ ,  $i_j \in \{[1, 2n], i_j \neq m, \ell\}$ . The sign is determined by the exponent  $l$  referring to the number of loops (closed paths) in the digraph.

Exact computation beyond a few modes is infeasible due to factorial growth of the number of digraphs  $N_g = (2n)!$ . Even the minimal cases considered here are challenging. However, truncating the sum to the most relevant digraphs offers insights into the dominant mixing processes responsible for non-reciprocity.

### 1. The isolator

To explain the non-reciprocal scattering of the isolator one has to consider at least three modes: the two modes  $\omega_a = \omega_0$  and  $\omega_b = \omega_0 + 2\Delta$ , and an auxiliary mode  $\omega_d = \omega_0 - \Delta$ . The two high-frequency pumps couple modes symmetrically around half their pump frequency by coupling their respective anti-modes, while the low-frequency pump couples modes separated by the pump's frequency, as shown in Fig. 3(a)].

The dynamics of the three modes is described by the  $6 \times 6$  matrix  $\mathbf{M}$ . An analytical approach using Eq. (A6) would involve  $N_g = 6! = 720$  digraphs. We distinguish two independent subsets that are not coupled to each other: the set of equations of modes  $a_a$ ,  $a_b$ , and anti-mode  $a_d^*$  and the set of equations of anti-modes  $a_a^*$ ,  $a_b^*$ , and mode  $a_d$ . By focusing on one subset, the dimensionality of the problem reduces, simplifying  $\mathbf{M}$  to

$$\mathbf{M} = \begin{pmatrix} -\Delta_d^* & g_1 & g_2 \\ -g_1^* & \Delta_a & g_3 \\ -g_2^* & g_3^* & \Delta_b \end{pmatrix}. \quad (\text{A7})$$

In Fig. 3(b) we use Eq. (A7) to graphically compute the digraphs contributing to the scattering terms  $S_{ab}$  and

$S_{ba}$ . For consistency with our experimental setup, we assume equal pump strengths  $|g_1| = |g_2| = g$  for the high-frequency pumps and a relative value  $|g_3| = rg$  for the low-frequency pump, with  $r \in \mathbb{R}$ . The mode couplings become  $g_1 = ge^{i\phi_1}$ ,  $g_2 = ge^{i\phi_2}$  and  $g_3 = rge^{i\phi_3}$ , resulting in

$$S_{ab} = \frac{i\gamma}{|M|} (g^2 e^{-i\phi_2} e^{i\phi_1} - rge^{-i\phi_3} \Delta_d^*), \quad (\text{A8})$$

$$S_{ba} = \frac{i\gamma}{|M|} (g^2 e^{i\phi_2} e^{-i\phi_1} - rge^{i\phi_3} \Delta_d^*). \quad (\text{A9})$$

Imposing  $S_{ab} = 0$  and assuming  $\Delta_d^* = \kappa_d e^{-i\alpha_d}$ , we derive the equation

$$g^2 e^{-i\phi_2} e^{i\phi_1} = rge^{-i\phi_3} \kappa_d e^{-i\alpha_d}. \quad (\text{A10})$$

We then retrieve the conditions

$$g^2 = rg\kappa_d \equiv \rho, \quad (\text{A11})$$

$$\phi_{loop} = -\alpha_d \quad (\text{A12})$$

where  $\phi_{loop} = \phi_1 - \phi_2 + \phi_3$  is the total phase of the loop among the three pumps, as shown in blue in Fig. 3(a). In our experiment we set  $\phi_1 = \phi_2$ , leading to  $\phi_3 = -\alpha_d$ . Plugging the conditions (A11) and (A12) into Eq. (A9) we find

$$S_{ba} \propto \rho (1 - e^{-2i\alpha_d}) \neq 0, \quad (\text{A13})$$

which is generally non-zero, as  $\alpha_d \neq 0$  due to the presence of losses and coupling in our transmission line setup ( $\gamma \neq 0$ ), proving non-reciprocity since  $S_{ab} = 0$ ,  $S_{ba} \neq 0$ .

Finally, adding mode  $\omega_e = \omega_0 + \Delta$  does not alter the validity of the results but would increase the dimensionality of  $\mathbf{M}$  and the number of digraphs. However, it is always possible to retrieve an approximate expression for  $S_{ab}$  and  $S_{ba}$  identical to Eqs. (A8) and (A9) by truncating the digraph expansion to the second order in pump power  $g$ , adopting the same approach shown for the circulator case below.

## 2. The circulator

The minimum number of modes to explain the non-reciprocal scattering of the circulator discussed in this paper is  $n = 5$  [see Fig. 4(a)]. With five modes, the total number of digraphs is  $N_g = (2 \cdot 5)! = 362880$ . However, in this case, the pumping scheme involves only low-frequency pumps  $\Omega_1 = \Delta$  and  $\Omega_2 = 2\Delta$  rendering the set of equations of motion of modes  $a_m$  and anti-modes  $a_m^*$  completely decoupled to each other. Without loss of precision, one can therefore half the number of equations. The matrix  $\mathbf{M}$  restricted only to the modes becomes

$$\mathbf{M} = \begin{pmatrix} \Delta_a & g_2 & g_1 & & \\ g_2^* & \Delta_d & g_2 & g_1 & \\ g_1^* & g_2^* & \Delta_b & g_2 & g_1 \\ & g_1^* & g_2^* & \Delta_e & g_2 \\ & & g_1^* & g_2^* & \Delta_c \end{pmatrix} \quad (\text{A14})$$

The total number of digraphs is now significantly reduced to  $N_g = 5! = 120$ , but the full analytical method is still largely impractical. Let us redefine the coupling of the pumps as  $g_1 = ge^{i/\phi_1}$  and  $g_2 = rge^{i/\phi_2}$  with  $r = \frac{|g_1|}{|g_2|} \in \mathbb{R}$ . Within the linear approximation used in this work, we assume both  $|g_1|, |g_2| \ll 1$ , which implies  $g \ll 1$ . We use the analytical Cramer method to estimate the approximate expressions of the matrix elements  $S_{ab}$  and  $S_{ba}$  by truncating the sum over the digraphs at second order in pump power  $g$ .

$$S_{ab} \simeq \frac{i\gamma}{|M|} (ge^{-i\phi_1} \Delta_d \Delta_e \Delta_c + r^2 g^2 e^{-i2\phi_2} \Delta_e \Delta_c + o(g^3)) \quad (\text{A15})$$

$$S_{ba} \simeq \frac{i\gamma}{|M|} (ge^{i\phi_1} \Delta_d \Delta_e \Delta_c + r^2 g^2 e^{i2\phi_2} \Delta_e \Delta_c + o(g^3)) \quad (\text{A16})$$

Figure 4(b) shows the relevant digraphs participating in the expression of  $S_{ab}$  and  $S_{ba}$ . Asking for  $S_{ab} = 0$  leads to the condition

$$ge^{-i\phi_1} \kappa_d e^{i\alpha_d} = r^2 g^2 e^{-i2\phi_2} \quad (\text{A17})$$

where we assume  $\Delta_d = \kappa_d e^{i\alpha_d}$  as for the isolator case. Equation (A17) leads to the conditions

$$g\kappa_d = r^2 g^2 \equiv \rho, \quad \phi_{loop} = -\alpha_d \quad (\text{A18})$$

where  $\phi_{loop} = 2\phi_2 - \phi_1$  is the total phase of the loop between the three interfering pumps shown in blue in Fig. 4(a). Inserting (A18) into (A16) and setting  $\phi_1 = 0$  to match our experiment conditions we get

$$S_{ba} \propto \rho (e^{i\alpha_d} - e^{-i\alpha_d}) = 2i\rho \sin \alpha_d \neq 0, \quad (\text{A19})$$

which is generally different from zero as  $\alpha_d \neq 0$  for finite coupling  $\gamma$ . We have thus proved the non-reciprocal scattering between modes  $a$  and  $b$ . Non-reciprocity between modes  $c$  and  $b$  follows by symmetry of the coupling scheme.

The non-reciprocity between the elements  $S_{ac}$  and  $S_{ca}$  is less obvious. As direct coupling between modes  $a$  and  $c$  is missing in the considered pumping scheme, the explanation requires extending the digraph expansion to terms  $O(g^3)$ .

$$S_{ac} \simeq \frac{i\gamma}{|M|} (-g^2 e^{-2i\phi_1} \Delta_d \Delta_e + r^2 g^3 e^{-i\phi_1} e^{-2i\phi_2} (\Delta_d + \Delta_b + \Delta_e) + o(g^4)) \quad (\text{A20})$$

$$S_{ca} \simeq \frac{i\gamma}{|M|} (-g^2 e^{2i\phi_1} \Delta_d \Delta_e + r^2 g^3 e^{i\phi_1} e^{2i\phi_2} (\Delta_d + \Delta_b + \Delta_e) + o(g^4)) \quad (\text{A21})$$

Forcing  $S_{ca} = 0$  leads to the condition

$$g^2 e^{2i\phi_1} \kappa_{de} e^{i\alpha_{de}} = r^2 g^3 e^{i\phi_1} e^{2i\phi_2} \kappa_T e^{i\alpha_T} \quad (\text{A22})$$

where we define  $\Delta_d \Delta_e = \kappa_{de} e^{i\alpha_{de}}$  and  $\Delta_d + \Delta_b + \Delta_e = \kappa_T e^{i\alpha_T}$ . Reshuffling the equation we obtain

$$g^2 \kappa_{de} e^{i(2\phi_2 - \phi_1)} = r^2 g^3 \kappa_T e^{i(\alpha_T - \alpha_{de})} \quad (\text{A23})$$

which leads to the conditions

$$g^2 \kappa_{de} = r^2 g^3 \kappa_T \equiv \rho' \quad (\text{A24})$$

$$\phi_{loop} = -(\alpha_T - \alpha_{de}) \quad (\text{A25})$$

It is straightforward to see that when condition (A25) is met  $S_{ac} \neq 0$ . Furthermore, if  $\alpha_T - \alpha_{de} \approx \alpha_d$  condition (A25) coincides with condition (A18) that sets  $S_{ab} \simeq 0$ . This confirms  $S_{ab} = S_{bc} \simeq S_{ca} \simeq 0$  yielding full circulation.

- 
- [1] M. H. Devoret and R. J. Schoelkopf. Superconducting Circuits for Quantum Information: An Outlook. *Science*, 339(6124):1169–1174, 2013.
  - [2] Xiu Gu, Anton Frisk Kockum, Adam Miranowicz, Yuxi Liu, and Franco Nori. Microwave photonics with superconducting quantum circuits. *Physics Reports*, 718-719:1–102, 2017.
  - [3] Frank Arute, Kunal Arya, Ryan Babbush, Dave Bacon, Joseph C. Bardin, Rami Barends, Rupak Biswas, Sergio Boixo, Fernando G. S. L. Brandao, David A. Buell, Brian Burkett, Yu Chen, Zijun Chen, Ben Chiaro, Roberto Collins, William Courtney, Andrew Dunsworth, Edward Farhi, Brooks Foxen, Austin Fowler, Craig Gidney, Marissa Giustina, Rob Graff, Keith Guerin, Steve Habegger, Matthew P. Harrigan, Michael J. Hartmann, Alan Ho, Markus Hoffmann, Trent Huang, Travis S. Humble, Sergei V. Isakov, Evan Jeffrey, Zhang Jiang, Dvir Kafri, Kostyantyn Kechedzhi, Julian Kelly, Paul V. Klimov, Sergey Knysh, Alexander Korotkov, Fedor Kostritsa, David Landhuis, Mike Lindmark, Erik Lucero, Dmitry Lyakh, Salvatore Mandrà, Jarrod R. McClean, Matthew McEwen, Anthony Megrant, Xiao Mi, Kristel Michielsen, Masoud Mohseni, Josh Mutus, Ofer Naaman, Matthew Neeley, Charles Neill, Murphy Yuezhen Niu, Eric Ostby, Andre Petukhov, John C. Platt, Chris Quintana, Eleanor G. Rieffel, Pedram Roushan, Nicholas C. Rubin, Daniel Sank, Kevin J. Satzinger, Vadim Smelyanskiy, Kevin J. Sung, Matthew D. Trevithick, Amit Vainsencher, Benjamin Villalonga, Theodore White, Z. Jamie Yao, Ping Yeh, Adam Zalcman, Hartmut Neven, and John M. Martinis. Quantum supremacy using a programmable superconducting processor. *Nature*, 574(7779):505–510, 2019.
  - [4] András Gyenis, Agustin Di Paolo, Jens Koch, Alexandre Blais, Andrew A. Houck, and David I. Schuster. Moving beyond the Transmon: Noise-Protected Superconducting Quantum Circuits. *PRX Quantum*, 2(3):030101, 2021.
  - [5] Joseph C. Bardin, Daniel H. Slichter, and David J. Reilly. Microwaves in Quantum Computing. *IEEE Journal of Microwaves*, 1(1):403–427, January 2021. Conference Name: IEEE Journal of Microwaves.
  - [6] Carlton M. Caves, Joshua Combes, Zhang Jiang, and Shashank Pandey. Quantum limits on phase-preserving linear amplifiers. *Physical Review A*, 86(6):063802, 2012.
  - [7] B. Yurke, M. L. Roukes, R. Movshovich, and A. N. Pargellis. A low-noise series-array Josephson junction parametric amplifier. *Applied Physics Letters*, 69(20):3078–3080, 1996.
  - [8] M. A. Castellanos-Beltran and K. W. Lehnert. Widely tunable parametric amplifier based on a superconducting quantum interference device array resonator. *Applied Physics Letters*, 91(8):083509, 2007.
  - [9] M. A. Castellanos-Beltran, K. D. Irwin, G. C. Hilton, L. R. Vale, and K. W. Lehnert. Amplification and squeezing of quantum noise with a tunable Josephson metamaterial. *Nature Physics*, 4(12):929–931, 2008.
  - [10] T. Yamamoto, K. Inomata, M. Watanabe, K. Matsuba, T. Miyazaki, W. D. Oliver, Y. Nakamura, and J. S. Tsai. Flux-driven Josephson parametric amplifier. *Applied Physics Letters*, 93(4):042510, 2008.
  - [11] N. Bergeal, F. Schackert, M. Metcalfe, R. Vijay, V. E. Manucharyan, L. Frunzio, D. E. Prober, R. J. Schoelkopf, S. M. Girvin, and M. H. Devoret. Phase-preserving amplification near the quantum limit with a Josephson ring modulator. *Nature*, 465(7294):64–68, 2010.
  - [12] Jose Aumentado. Superconducting Parametric Amplifiers: The State of the Art in Josephson Parametric Amplifiers. *IEEE Microwave Magazine*, 21(8):45–59, 2020.
  - [13] Baleegh Abdo, Katrina Sliwa, Luigi Frunzio, and Michel Devoret. Directional Amplification with a Josephson Circuit. *Physical Review X*, 3(3):031001, 2013.
  - [14] A. Metelmann and A. A. Clerk. Nonreciprocal Photon Transmission and Amplification via Reservoir Engineering. *Physical Review X*, 5(2):021025, 2015.
  - [15] C. Macklin, K. O’Brien, D. Hover, M. E. Schwartz, V. Bolkhovskiy, X. Zhang, W. D. Oliver, and I. Siddiqi. A near-quantum-limited Josephson traveling-wave parametric amplifier. *Science*, 350(6258):307–310, 2015.
  - [16] Hampus Renberg Nilsson, Anita Fadavi Roudsari, Daryoush Shiri, Per Delsing, and Vitaly Shumeiko. High-Gain Traveling-Wave Parametric Amplifier Based on Three-Wave Mixing. *Physical Review Applied*, 19(4):044056, 2023.
  - [17] Archana Kamal, John Clarke, and M. H. Devoret. Noiseless non-reciprocity in a parametric active device. *Nature Physics*, 7(4):311–315, 2011.
  - [18] Nicholas A. Estep, Dimitrios L. Sounas, Jason Soric, and Andrea Alù. Magnetic-free non-reciprocity and isolation based on parametrically modulated coupled-resonator loops. *Nature Physics*, 10(12):923–927, 2014.
  - [19] Joseph Kerckhoff, Kevin Lalumière, Benjamin J. Chapman, Alexandre Blais, and K. W. Lehnert. On-Chip Superconducting Microwave Circulator from Synthetic Rotation. *Physical Review Applied*, 4(3):034002, 2015.



- [20] Arkady Fedorov, N. Pradeep Kumar, Dat Thanh Le, Rohit Navarathna, Prasanna Pakkiam, and Thomas M. Stace. Nonreciprocity and Circulation in a Passive Josephson-Junction Ring. *Physical Review Letters*, 132(9):097001, 2024.
- [21] F. Lecocq, L. Ranzani, G. A. Peterson, K. Cicak, R. W. Simmonds, J. D. Teufel, and J. Aumentado. Non-reciprocal Microwave Signal Processing with a Field-Programmable Josephson Amplifier. *Physical Review Applied*, 7(2):024028, 2017.
- [22] F. Lecocq, L. Ranzani, G.A. Peterson, K. Cicak, A. Metelmann, S. Kotler, R.W. Simmonds, J.D. Teufel, and J. Aumentado. Microwave Measurement beyond the Quantum Limit with a Nonreciprocal Amplifier. *Physical Review Applied*, 13(4):044005, 2020.
- [23] F. Lecocq, L. Ranzani, G. A. Peterson, K. Cicak, X. Y. Jin, R. W. Simmonds, J. D. Teufel, and J. Aumentado. Efficient Qubit Measurement with a Nonreciprocal Microwave Amplifier. *Physical Review Letters*, 126(2):020502, 2021.
- [24] L. Deák and T. Fülöp. Reciprocity in quantum, electromagnetic and other wave scattering. *Annals of Physics*, 327(4):1050–1077, 2012.
- [25] Leonardo Ranzani and José Aumentado. Graph-based analysis of nonreciprocity in coupled-mode systems. *New Journal of Physics*, 17(2):023024, 2015.
- [26] Mats O. Tholén, Riccardo Borgani, Giuseppe Ruggero Di Carlo, Andreas Bengtsson, Christian Krizan, Marina Kudra, Giovanna Tancredi, Jonas Bylander, Per Delsing, Simone Gasparinetti, and David B. Haviland. Measurement and control of a superconducting quantum processor with a fully integrated radio-frequency system on a chip. *Review of Scientific Instruments*, 93(10):104711, 2022.
- [27] Ofer Naaman and José Aumentado. Synthesis of Parametrically Coupled Networks. *PRX Quantum*, 3(2):020201, 2022.
- [28] J. C. Rivera Hernández, Fabio Lingua, Shan W. Jolin, and David B. Haviland. Control of multi-modal scattering in a microwave frequency comb. *APL Quantum*, 1(3):036101, 2024.
- [29] Leonardo Ranzani and Jose Aumentado. Circulators at the Quantum Limit: Recent Realizations of Quantum-Limited Superconducting Circulators and Related Approaches. *IEEE Microwave Magazine*, 20(4):112–122, 2019.